PCCP

PAPER



Cite this: *Phys. Chem. Chem. Phys.*, 2018, **20**, 22972

# AA- and ABA-stacked carbon nitride ($C_3N_4$): novel photocatalytic water splitting solar-to-hydrogen energy conversion

A. H. Reshak [abc]

Received 7th May 2018,
Accepted 15th August 2018

DOI: 10.1039/c8cp02898b

rsc.li/pccp

We report the development of the $C_3N_4$ structure by integrating two different structures: (i) two identical layers as AA-stacked $C_3N_4$ and (ii) intercalating one different layer between two identical layers as ABA-stacked $C_3N_4$. This in turn endows $C_3N_4$ with significantly promoted charge migration, up-shifted conduction-band (CB) level, enhanced CB potential from −0.89 eV (AA-stacked $C_3N_4$) to −1.03 eV (ABA-stacked $C_3N_4$), broadened band gap as well as enhanced surface area, all of which favor the enhancement of the photocatalytic performance. The optical absorption level exhibited significant enhancement in the visible light region when shifting from AA-stacked $C_3N_4$ to ABA-stacked $C_3N_4$, where the absorption edge moves from $\lambda$ = 508.1 → $\lambda$ = 454.1 nm. This corresponds to the direct optical band gap of 2.44 eV → 2.73 eV, which is well matched with the solar spectrum and the sufficient negative CB potential for $H^+/H_2$ reduction. Based on these results, we can conclude that AA-stacked and ABA-stacked $C_3N_4$ satisfies all the requirements to be efficient photocatalysts. This study will significantly improve the search efficiency and considerably aid the experimentalists in the exploration of novel photocatalysts.

## 1. Introduction

Carbon nitride ($C_3N_4$) has gained considerable interest as a potential candidate for various technological applications.[1–14] Metal-free graphitic carbon nitride (g-$C_3N_4$) shows tremendous potentials in energy and environmental applications. Nonetheless, amelioration on the crystal configuration, electronic structure and microstructure of $C_3N_4$ for high-performing visible-light (VIS) photocatalysis is still challenging. Wang *et al.*[15] reported that g-$C_3N_4$ is a metal free photocatalyst that can absorb VIS due to its band gap (2.70 eV), which is well matched with the solar spectrum and possesses sufficiently negative conduction band (CB) potential for $H^+/H_2$ reduction. It also has high chemical stability, extraordinary optical characteristics and good thermal solidity, which make g-$C_3N_4$ an active photocatalyst under VIS irradiation. The electrochemical properties of tubular g-$C_3N_4$ were investigated,[16,17] and it has been reported that the tubular g-$C_3N_4$ shows high suitability as a photocatalyst and supercapacitor. The improvement in the performance of g-$C_3N_4$ is due to its high surface area that includes more active sites for reaction. The phenomenon of absorbing electromagnetic radiation is very important for photocatalysts to be used for environment remediation and energy storage purposes. $C_3N_4$ with its high stability and reasonable band gap has been a fascinating research topic for theorists and as well as experimentalists. Graphitic carbon nitride (g-$C_3N_4$), as a nontoxic metal-free and easily available layered material, shows high capabilities of photocatalytic hydrogen evolution,[15] contaminant elimination[10] and $CO_2$ reduction.[18] Nonetheless, the photocatalytic performance of g-$C_3N_4$ is limited by the low quantum efficiency derived from its slow charge mobility and fast recombination of charge carriers. To resolve these drawbacks, various attempts have been made, such as building sundry nanoarchitectures,[19] surface modification,[20] fabrication of heterojunction[21] and doping with chemical elements.[22–28] Herein, we report the development of a $C_3N_4$ structure using (i) two identical layers of $C_3N_4$ as AA-stacked $C_3N_4$ and (ii) intercalating one different layer between two identical layers as ABA-stacked $C_3N_4$. This in turn endows $C_3N_4$ with significantly promoted charge migration, up-shifted CB level, enhanced potential of CB from −0.89 eV (AA-stacked $C_3N_4$) to − 1.03 eV (ABA-stacked $C_3N_4$), broadened band gap as well as enhanced surface area. We should emphasize that the layer structure favors the enhancement of the photocatalytic performance.[29]

It is well known that the first-principles calculations have the capability to precisely predict the properties of the materials,

[a] *New Technologies – Research Center, University of West Bohemia, Univerzitni 8, 306 14 Pilsen, Czech Republic. E-mail: maalidph@yahoo.co.uk; Tel: +420 777729583*
[b] *Nanotechnology and Catalysis Research Center (NANOCAT), University of Malaya, 50603 Kuala Lumpur, Malaysia*
[c] *Department of Instrumentation and Control Engineering, Faculty of Mechanical Engineering, CTU in Prague, Technicka 4, 166 07 Prague 6, Czech Republic*

which helps to design new materials with novel properties. This significantly helps the experimentalists in the exploration of novel materials with excellent properties.[30–34] Recently, density functional theory (DFT) approaches have been used to explore new photocatalysts with efficient photocatalytic performance, which agree well with the experimental data.[32–43] In this study, we will concentrate on the photocatalytic activity of AA- and ABA-stacked $C_3N_4$ as novel, green and efficient photocatalysts. This is a natural extension to our previous study on calculating the electronic structure, linear and nonlinear optical properties and the thermoelectric properties of the same materials.[44–46] In our previous study[37] we reported the development of chlorine (Cl)-intercalated g-$C_3N_4$ *via* co-pyrolysis of melamine and excess ammonium chloride for water splitting to produce $H_2$, $CO_2$ reduction, and removal of liquid and air contaminants.[47]

## 2. Methodology aspect

DFT calculations were performed to investigate the suitability of AA- and ABA-stacked $C_3N_4$ to be used as active photocatalysts in the VIS region. The structures of AA- and ABA-stacked $C_3N_4$ are stable in hexagonal symmetry.[4] For more details about the structure information of AA- and ABA-stacked $C_3N_4$, we refer the readers to ref. 4 and our previous studies.[44–46] The full-potential augmented plane wave plus local orbitals (FPLAPW + lo) based on the DFT within the framework of wien2k package[48] was used. The self-consistent calculations were achieved using generalized gradient approximation (PBE − GGA),[49] and the ground state properties were obtained by using the recently modified Becke–Johnson potential scheme (mBJ).[50] For the convergence of energy eigenvalues, the wave function in the interstitial regions were expended in plane waves with cutoff $R_{MT}K_{max}$ = 7.0, where $R_{MT}$ and $K_{max}$ stand for the muffin-tin (MT) sphere radius and magnitude of the largest $K$ vector in plane wave expansion, respectively. The chosen $R_{MT}$ value was 1.24 atomic units (a.u.) for C and N atoms for both AA- and ABA-stacked $C_3N_4$. The wave function inside the sphere was expended up to $l_{max}$ = 10, whereas the Fourier expansion of the charge density was up to $G_{max}$ = 12 (a.u.)$^{-1}$. The self-consistent calculations were converged with the difference in total energy of the crystal that did not exceed $10^{-5}$ Ryd for successive steps. The self-consistent calculations were obtained for both cases by using 5000k points in the irreducible Brillouin zone (IBZ).

## 3. Results and discussion

### 3.1. Structure–property

The schematics of charge transfer and the photocatalytic mechanism of AA- and ABA-stacked $C_3N_4$ are shown in Fig. 1. It is clearly seen that the photogenerated electron and hole ($e^-$–$h^+$) pairs are produced when the photocatalyst absorbs radiation. This stage is referred to as the semiconductor's photo-excitation state. The proton ($H^+$) assisted the multi-electron processes for $CO_2$ photoreduction,[51,52] while the photoexcited $e^-$ can react with surface adsorbed $CO_2$ in the presence of $H^+$ (produced in water oxidation) to evolve $CH_4$ as a primary product. Moreover, the generated $h^+$ are involved in water oxidation, producing $O_2$ and $H^+$.[51,52]

We used the calculated electronic band structure (Fig. 2a and b) to explore the photocatalytic performance[53] of AA-/ABA-stacked $C_3N_4$. Fig. 2a and b clearly show that the conduction band minimum (CBM) and the valence band maximum (VBM) are located at $A$ point for AA-stacked $C_3N_4$ and at $\Gamma$ point for ABA-stacked $C_3N_4$, resulting in a direct band gap ($E_g$). The calculated value of the fundamental $E_g$ is about 2.589 eV (AA-stacked $C_3N_4$) and 2.990 eV (ABA-stacked $C_3N_4$). It is interesting to highlight that the N 2p orbital is dominant and plays a major role in formation of the VBM, while the CBM is mainly derived from hybridized C 2p and N 2p orbitals. The valence band is fashioned by hybridized C 2p and N 2p with a small component of C 2s and N 2s. We can also see strong hybridization between C 2s and N 2s states and C 2p and N 2p states, which favors the enhancement of covalent bonding as can be observed from electronic charge density contours. Covalent bonding is more favorable for efficient carriers' transportation than ionic bonding.[54] The C–C and C–N bonds possess strong electron cloud overlap and prefer to attract $h^+$ and

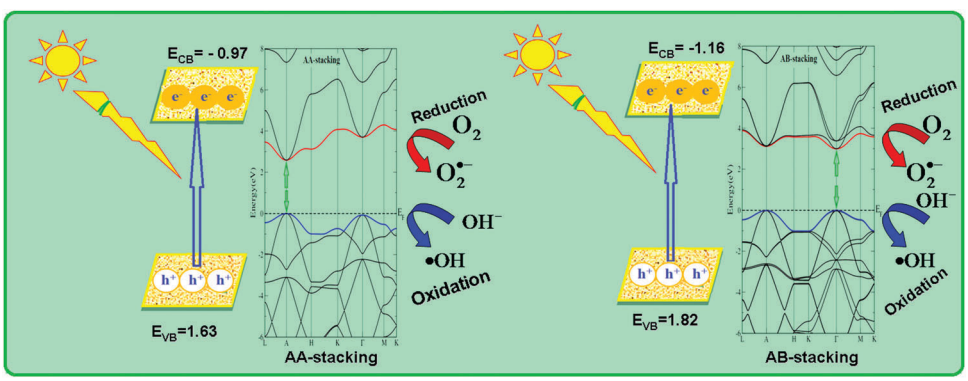


Fig. 1 The schematics of charge transfer and photocatalytic mechanism of AA- and ABA-stacked $C_3N_4$. When a photocatalyst absorbs radiation from sunlight, it produces electron and hole pairs. The electron of the valence band becomes excited when illuminated by light. The excess energy of this excited electron promoted the electron to the conduction band therefore, creating the negative electron ($e^-$) and positive hole ($h^+$) pair. This stage is referred as the semiconductor's 'photo-excitation' state.

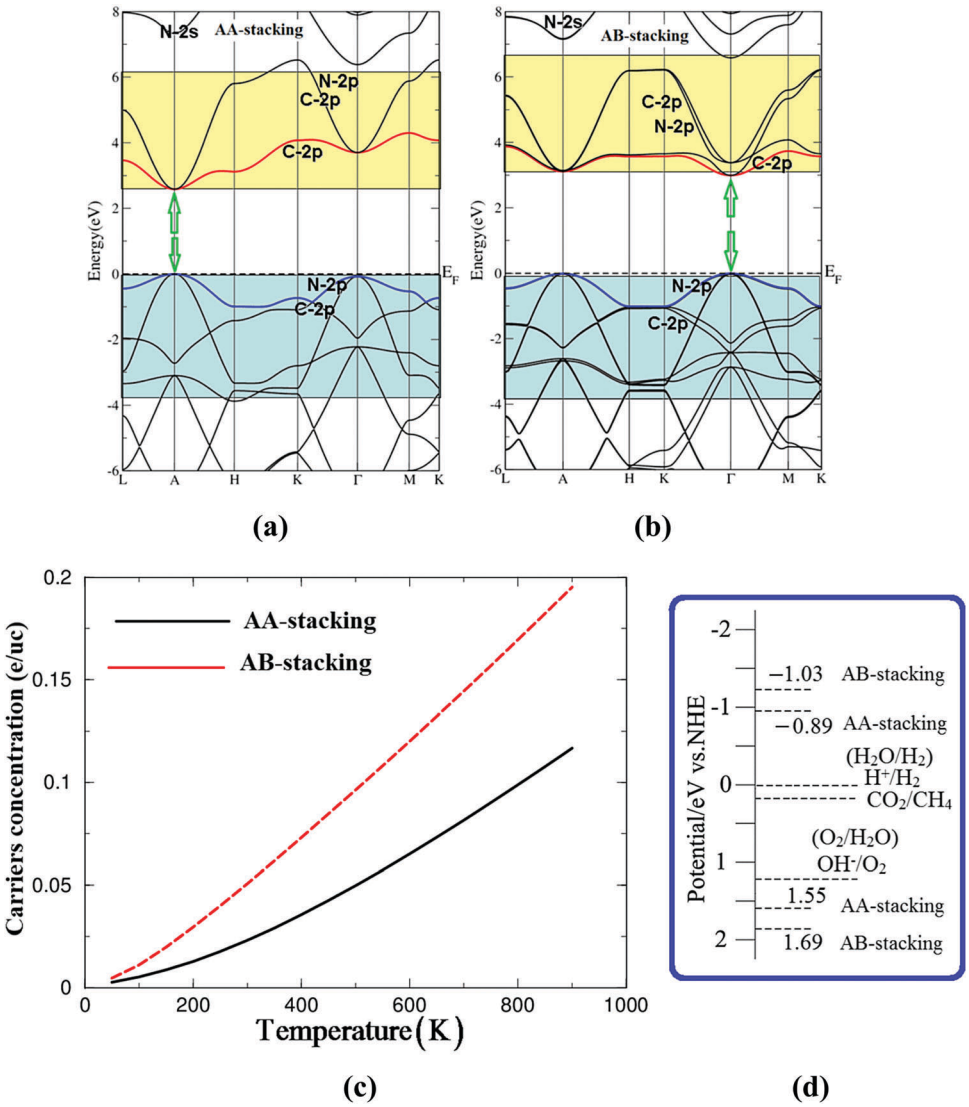


Fig. 2 (a and b) The calculated electronic band structure of AA- and ABA-stacked $C_3N_4$. (c) The carriers' concentration of AA- and ABA-stacked $C_3N_4$. (d) The schematics of potential in eV *vs.* NHE for AA- and ABA-stacked $C_3N_4$.

repel $e^-$, thus facilitating separation of the $e^- - h^+$ pairs. This in turn enhances the photocatalytic performance.[55]

Fig. 2a and b show that the bands at around the Fermi level ($E_F$) possess low effective masses ($m_e$* and $m_h$*), resulting in high-mobility carriers (Table 1), which enhance the charge transfer process. The photogenerated carriers with high mobility also enhance the photocatalytic activity.[56,57] Moreover, the great effective mass difference ($D = m_e^*/m_h^*$), as shown in Table 1, can assist the $e^-$ and $h^+$ migration and separation and finally improve the photocatalytic activity. It is clearly seen from Table 1 that $m_h^* > m_e^*$, resulting in a significant difference in the mobility between $e^-$ and $h^+$. The mobility of $e^-$ and $h^+$ can be indirectly assessed by their $m_e^*$ and $m_h^*$ following the expression ($(\text{mobility})_e = e\tau_e/m_e^*$ and $(\text{mobility})_h = e\tau_h/m_h^*$). The large mobility difference is useful in the separation of $e^-$ and $h^+$, reduction of $e^-$ and $h^+$ recombination rate, and improvement of the photocatalytic performance. Moreover, it is clear from Table 1 that $m_e^*$ and $m_h^*$ are small; thus, we can deduce that the $e^-$ and $h^+$ transfer can be fast along different directions.

Table 1 Calculated effective masses

| Effective mass | AA-stacked $C_3N_4$ | AB-stacked $C_3N_4$ |
|---|---|---|
| $m_e^*/m_o$ | 0.02047 | 0.02497 |
| $m_{hh}^*/m_o$ | 0.03609 | 0.03547 |
| $m_{lh}^*/m_o$ | 0.00802 | 0.00757 |
| $D = m_{hh}^*/m_e^*$ | 1.76306 | 1.42050 |
| $D = m_e^*/m_{hh}^*$ | 0.56719 | 0.70397 |
| $D = m_{lh}^*/m_e^*$ | 0.39179 | 0.30316 |
| $D = m_e^*/m_{lh}^*$ | 2.55238 | 3.29858 |

The other crucial issue to understand the photocatalytic mechanism in AA-/ABA-stacked $C_3N_4$ is the carriers' concentration ($n$) and their mobility. Thus, we investigated the influence of temperature ($T$) on $n$ at a certain value of the chemical potential ($\mu = E_F$), as shown in Fig. 2c. We can see that $n$ increases almost

 

linearly with the increase in $T$. We should highlight that the carriers' concentration was obtained from the ground state within the limits of Boltzmann theory[58–60] and the constant relaxation time approximation, as implemented in the BoltzTraP code.[61]

The photocatalytic oxidation is mainly attributed to the participation of $O_2^{\bullet -}$, $^{\bullet}OH$ and the photogenerated $h^+$[62] (Fig. 1). In order to understand the photocatalytic mechanism of AA- and ABA-stacked $C_3N_4$, the reduction and oxidation potentials of the CBM and the VBM at the point of zero charge can be calculated using the equations taken from ref. 63:

$$E_{CB} = \chi - E^C - (E_g/2) \quad (1)$$

$$E_{VB} = E_{CB} + E_g \quad (2)$$

The $E_{CB}$ and $E_{VB}$ values of AA- and ABA-stacked $C_3N_4$ are shown in Fig. 2d. This figure illustrates the probable energy level diagram (potential *vs.* NHE) and $CO_2$ photoreduction, displaying the relative positions of CB and VB for AA- and ABA-stacked $C_3N_4$, and redox potentials for $CO_2/CH_4$ and $O_2/H_2O$. AA-stacked $C_3N_4$ appears to be a more efficient photocatalyst for $CO_2$ photoreduction, possessing a CBM at −0.89 eV, and a corresponding VBM at 1.55 eV. The CBM lies above the redox potential of $CO_2/CH_4$ (0.17 eV), whereas the VBM lies above the $O_2/H_2O$ redox potential (1.23 eV).[52] It can be clearly seen that the CB edge potential of ABA-stacked $C_3N_4$ is more negative than that of AA-stacked $C_3N_4$, indicating that the ABA-stacked $C_3N_4$ has stronger reduction power for $H_2$ production than the AA-stacked $C_3N_4$. A semiconductor with a more negative CB edge potential has stronger reduction power for $H_2$ production from water.[64–67] According to the results shown in Fig. 2d, AA- and ABA-stacked $C_3N_4$ possess high negative reduction potential of excited electrons due to their higher CB position and hence, the location of the CBM and VBM accommodates the redox capacity.

### 3.2. Photo-electrochemical properties

The free radicals $O_2^{\bullet -}$ and $^{\bullet}OH$ with high oxidation ability can oxidize various organic and inorganic carbon compounds to produce carbon dioxide, water and other non-toxic small organic molecules. Hence, $E_g$ of the photocatalyst determines the range of the light absorbed (see Fig. 3a and b). The optical absorption induces the transfer of $e^-$ from the VB → CB, generating the $e^- - h^+$ pairs, which can then migrate to the surface to participate in oxidation and reduction reactions.[68,69] Usually the locations of the VBM and the CBM determine the oxidation and reduction capabilities of the photogenerated $e^-$ and $h^+$, respectively.[68] The reduction potential level of the $e^-$-acceptors should be energetically below the CBM, whereas the oxidization potential level of the $e^-$-donors should be above the VBM.[70] The optical $E_g$ value of the AA-stacked and ABA-stacked $C_3N_4$ can be estimated from the absorption spectrum, as shown in Fig. 3a and b. The square of the absorption coefficient $I(\omega)$ is linear with photon energy ($h\nu$) for direct optical transitions in the absorption edge region, whereas the square root of $I(\omega)$ is linear with $h\nu$ for indirect optical transitions.[32] The data plots of $[I(\omega)]^2$ *vs.* $h\nu$ in the absorption edge region are shown in the inset of Fig. 3a and b. It is clearly shown that $[I(\omega)]^2$ *vs.* $h\nu$ is linear in the absorption edge region. Therefore, the absorption edge of the AA-stacked and ABA-stacked $C_3N_4$ is caused by direct transitions. Furthermore, the absorption edge occurs at $\lambda$ = 508.1 nm (AA-stacked $C_3N_4$) and $\lambda$ = 454.1 nm (ABA-stacked $C_3N_4$) and the optical $E_g$ is estimated ($\lambda_g = 1239.8/E_{g(optical)}$[71]) to be 2.44 eV (AA-stacked $C_3N_4$) and 2.73 eV (ABA-stacked $C_3N_4$).

### 3.3. The electronic charge density and charge transfer relationship

The electronic charge density distribution of AA-stacked and ABA-stacked $C_3N_4$, which is derived from the reliable converged wave function,[72,73] were calculated and shown in Fig. 4 to investigate the $e^-$ and $h^+$ transfer. According to the Pauling scale, the low electro-negativity difference between C and N atoms points to an almost non-polar covalent bond with only 9% of ionic character.[74] It is clear that maximum charge is accumulated around C and N atoms, as indicated by the blue color. This implies that efficient charge transfer occurs towards

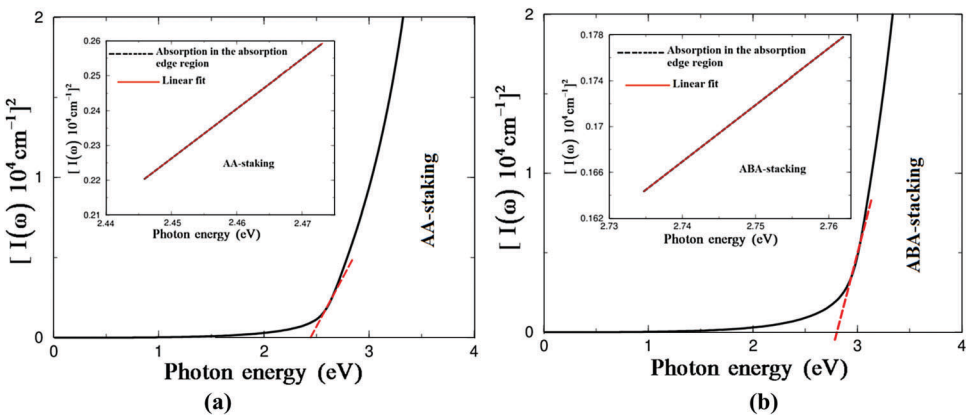


Fig. 3 (a and b) The data plots of $[I(\omega)]^2$ *versus* photon energy in the absorption edge region. From the absorption spectrum, the optical band gap value of the semiconductor can be solved as follows: the square of the absorption coefficient $I(\omega)$ is linear with photon energy for direct optical transitions in the absorption edge region. It is clearly shown that $[I(\omega)]^2$ *vs.* photon energy is linear in the absorption edge region. This plot suggests that the absorption edge of the investigated material is caused by direct transitions.

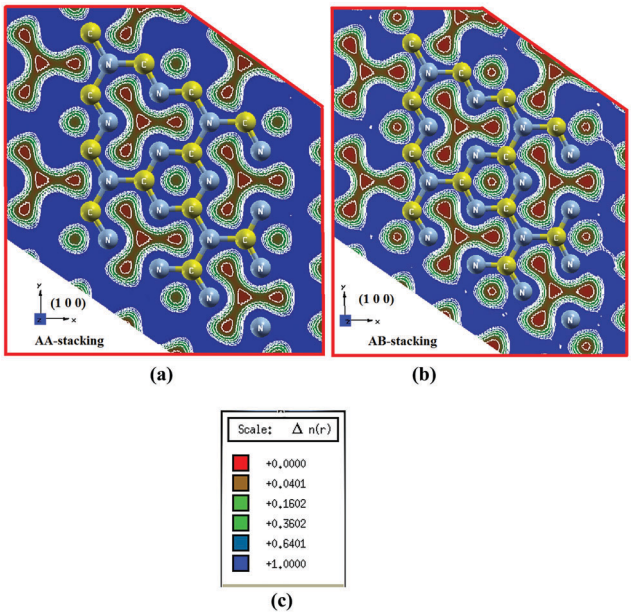


Fig. 4 (a and b) Calculated electronic charge density distribution which shows that C–C and C–N bonds possess strong electron cloud overlap and prefer to attract holes and repel electrons, thus facilitating separation of the photogenerated e–h pairs. This in turn enhances the photocatalytic activity; (c) thermoscale.

N atom due to the fact that the electro-negativity of N atom is larger than that of C atom. According to the thermo-scale (Fig. 4c), the blue color represents the maximum charge distribution and strong charge sharing between C and N atoms, resulting in strong covalent bonding, while the red color represents zero charge. Thus, the formation of AA-stacked and ABA-stacked $C_3N_4$ efficaciously extends the local 2D-conjugated system of g-$C_3N_4$ into 3D space and subsequently promotes the separation and mobility of charge carriers.

## 4. Conclusions

Two configurations of $C_3N_4$, namely, AA-stacked and ABA-stacked $C_3N_4$ are proposed to enhance the photocatalytic performance of $C_3N_4$ with significantly promoted charge migration, up-shifted CB level, enhanced CB potential, increased $E_g$ as well as enhanced surface area, all of which favor the enhancement of the photocatalytic performance. The calculated value of the fundamental $E_g$ is about 2.589 eV (AA-stacked $C_3N_4$) and 2.990 eV (ABA-stacked $C_3N_4$). The absorption edge occurs at $\lambda$ = 508.1 nm (AA-stacked $C_3N_4$) and $\lambda$ = 454.1 nm (ABA-stacked $C_3N_4$), which correspond to an optical $E_g$ of about 2.44 eV (AA-stacked $C_3N_4$) and 2.73 eV (ABA-stacked $C_3N_4$). The C–C and C–N bonds possess strong electron cloud overlap and prefer to attract $h^+$ and repel $e^-$, thus facilitating separation of the photogenerated $e^-$–$h^+$ pairs. This in turn enhances the photocatalytic activity. AA-stacked $C_3N_4$ appears to be a more efficient photocatalyst for $CO_2$ photoreduction, possessing a CBM at −0.89 eV and a corresponding VBM at 1.55 eV. The CBM bottom lies above the redox potential of $CO_2/CH_4$ (0.17 eV), whereas the VBM lies above the $O_2/H_2O$ redox potential (1.23 eV). It can be clearly seen that the CB edge potential of ABA-stacked $C_3N_4$ is more negative than that of AA-stacked $C_3N_4$, indicating that the ABA-stacked $C_3N_4$ has stronger reduction power for $H_2$ production than the AA-stacked $C_3N_4$. The suitable $E_g$ width and the appropriate CBM position together contribute to the optimal $H_2$ production activity under light illumination. Therefore, a balance between the light absorption capability and the reduction power leads to higher efficiency of light-driven photocatalytic $H_2$ production.

## Author contribution

A. H. Reshak, as a professor with PhD in physics and PhD in materials engineering has performed the calculations, analyzing and discussing the results and writing the manuscript.

## Conflicts of interest

The author declares no competing financial interests.

## Acknowledgements

This study was performed within the CENTEM project, reg. no. CZ.1.05/2.1.00/03.0088, CENTEM PLUS (LO1402). Computational resources were provided by MetaCentrum (LM2010005) and CERIT-SC (CZ.1.05/3.2.00/08.0144) infrastructures.

## References

1 E. Kroke and M. Schwarz, Novel group 14 nitrides, *Coord. Chem. Rev.*, 2004, **248**, 493.
2 M. H. V. Huynh, M. A. Hiskey, J. G. Archuleta and E. L. Roemer, Preparation of Nitrogen-Rich Nanolayered, Nanoclustered, and Nanodendritic Carbon Nitrides, *Angew. Chem., Int. Ed.*, 2004, **43**, 5658; 2005, 44, 737.
3 L. C. Ming, P. Zinin, Y. Meng, X. R. Liu, S. M. Hong and Y. Xie, A cubic phase of C3N4 synthesized in the diamond-anvil cell, *J. Appl. Phys.*, 2006, **99**, 033520.
4 D. M. Teter and R. J. Hemley, Low-compressibility carbon nitrides, *Science*, 1996, **271**, 53.
5 (*a*) A. Y. Liu and M. L. Cohen, Prediction of New Low Compressibility Solids, *Science*, 1989, **245**, 841; (*b*) A. Y. Liu and M. L. Cohen, Structural properties and electronic structure of low-compressibility materials: β-$Si_3N_4$ and hypothetical β-$C_3N_4$, *Phys. Rev. B: Condens. Matter Mater. Phys.*, 1990, **41**, 10727.
6 Q. Lv, C. B. Cao, C. Li, J. T. Zhang, H. S. Zhu, X. Kong and X. F. Duan, Formation of crystalline carbon nitride powder by a mild solvothermal method, *J. Mater. Chem.*, 2003, **13**, 1241.
7 D. R. Miller, D. C. Swenson and E. G. Gillan, Synthesis and Structure of 2,5,8-Triazido-*s*-Heptazine: An Energetic and Luminescent Precursor to Nitrogen-Rich Carbon Nitrides, *J. Am. Chem. Soc.*, 2004, **126**, 5372.

 

8 S. Melissen, T. L. Bahers, S. N. Steinmann and P. Sautet, Relationship between Carbon Nitride Structure and Exciton Binding Energies: A DFT Perspective, *J. Phys. Chem. C*, 2015, **119**, 25188–25196.

9 X. Chen, N. Li, Z. Kong, W.-J. Ong and X. Zhao, Photocatalytic Fixation of Nitrogen to Ammonia: State-of-the-Art Advancement and Future Prospects, *Mater. Horiz.*, 2018, **5**, 9–27.

10 W.-J. Ong, 2D/2D Graphitic Carbon Nitride (g-$C_3N_4$) Heterojunction Nanocomposites for Photocatalysis: Why Does Face-to-Face Interface Matter?, *Frontiers in Materials*, 2017, **4**, 11, DOI: 10.3389/fmats.2017.

11 D. Zeng, W.-J. Ong, H. Zheng, M. Wu, Y. Chen, D.-L. Peng and M.-Y. Han, $Ni_{12}P_5$ nanoparticles embedded into porous g-$C_3N_4$ nanosheets as a noble-metal-free hetero-structural photocatalyst for efficient H2 production under visible light, *J. Mater. Chem. A*, 2017, **5**, 16171–16178.

12 D. Zeng, W. Xu, W.-J. Ong, J. Xu, H. Ren, Y. Chen, H. Zheng and D.-L. Peng, Toward noble-metal-free visible-light-driven photocatalytic hydrogen evolution: Monodisperse sub-15 nm $Ni_2P$ nanoparticles anchored on porous g-$C_3N_4$ nanosheets to engineer 0D–2D heterojunction interfaces, *Appl. Catal., B*, 2018, **221**, 47–55.

13 N. Sun, Y. Liang, X. Ma and F. Chen, Reduced Oxygenated g-$C_3N_4$ with Abundant Nitrogen Vacancies for Visible-Light Photocatalytic Applications, *Chem. – Eur. J.*, 2017, **23**, 15466–15473.

14 Z. Pan, Y. Zheng, F. Guo, P. Niu and X. Wang, Decorating CoP and Pt Nanoparticles on Graphitic Carbon Nitride Nanosheets to Promote Overall Water Splitting by Conjugated Polymers, *ChemSusChem*, 2017, **10**, 87–90.

15 X. C. Wang, K. Maeda, A. Thomas, K. Takanabe, G. Xin, J. M. Carlsson, K. Domen and M. Antonietti, A metal-free polymeric photocatalyst for hydrogen production from water under visible light, *Nat. Mater.*, 2009, **8**, 76–80.

16 M. Tahir, C. Cao, F. K. Butt, F. Idrees, N. Mahmood, I. Aslam, Z. Ali, M. Tanvir, M. Rizwan and T. Mahmood, Tubular graphitic–$C_3N_4$: a prospective material for energy storage and green photocatalysis, *J. Mater. Chem. A*, 2013, **1**, 13949–13955.

17 X. C. Wang, X. F. Chen, A. Thomas, X. Z. Fu and M. Antonietti, Metal-Containing Carbon Nitride Compounds: A New Functional Organic–Metal Hybrid Material, *Adv. Mater.*, 2009, **21**, 1609–1612.

18 J. Mao, T. Y. Peng, X. H. Zhang, K. Li, L. Q. Ye and L. Zan, Effect of graphitic carbon nitride microstructures on the activity and selectivity of photocatalytic $CO_2$ reduction under visible light, *Catal. Sci. Technol.*, 2013, **3**, 1253–1260.

19 Y. Zheng, L. H. Lin, X. J. Ye, F. S. Guo and X. C. Wang, Helical Graphitic Carbon Nitrides with Photocatalytic and Optical Activities, *Angew. Chem., Int. Ed.*, 2014, **53**, 11926–11930.

20 M. Groenewolt and M. Antonietti, Synthesis of g-$C_3N_4$ Nanoparticles in Mesoporous Silica Host Matrices, *Adv. Mater.*, 2005, **17**, 1789–1792.

21 C. S. Pan, J. Xu, Y. J. Wang, D. Li and Y. F. Zhu, Dramatic Activity of $C_3N_4$/$BiPO_4$ Photocatalyst with Core/Shell Structure Formed by Self-Assembly, *Adv. Funct. Mater.*, 2012, **22**, 1518–1524.

22 S. C. Yan, Z. S. Li and Z. G. Zou, Photodegradation of Rhodamine B and Methyl Orange over Boron-Doped g-$C_3N_4$ under Visible Light Irradiation, *Langmuir*, 2010, **26**, 3894–3901.

23 Y. J. Zhang, T. Mori, J. H. Ye and M. Antonietti, Phosphorus-Doped Carbon Nitride Solid: Enhanced Electrical Conductivity and Photocurrent Generation, *J. Am. Chem. Soc.*, 2010, **132**, 6294–6295.

24 G. Liu, P. Niu, C. H. Sun, S. C. Smith, Z. G. Chen, G. Q. Lu and H. M. Cheng, Unique Electronic Structure Induced High Photoreactivity of Sulfur-Doped Graphitic $C_3N_4$, *J. Am. Chem. Soc.*, 2010, **132**, 11642–11648.

25 G. H. Dong, K. Zhao and L. Z. Zhang, Carbon self-doping induced high electronic conductivity and photoreactivity of g-$C_3N_4$, *Chem. Commun.*, 2012, **48**, 6178–6180.

26 J. H. Li, B. Shen, Z. H. Hong, B. Z. Lin, B. F. Gao and Y. L. Chen, A facile approach to synthesize novel oxygen-doped g-$C_3N_4$ with superior visible-light photoreactivity, *Chem. Commun.*, 2012, **48**, 12017–12019.

27 L. Xu, J. X. Xia, H. Xu, J. Qian, J. Yan, L. G. Wang, K. Wang and H. M. Li, AgX/graphite-like $C_3N_4$ (X = Br, I) hybrid materials for photoelectrochemical determination of copper(II) ion, *Analyst*, 2013, **138**, 6721–6726.

28 Q. Liu and J. Y. Zhang, Graphene Supported Co–g-$C_3N_4$ as a Novel Metal–Macrocyclic Electrocatalyst for the Oxygen Reduction Reaction in Fuel Cells, *Langmuir*, 2013, **29**, 3821–3828.

29 A. H. Reshak, Active Photocatalytic Water Splitting Solar-to-Hydrogen Energy Conversion: Chalcogenide Photocatalyst $Ba_2ZnSe_3$ under Visible Irradiation, *Appl. Catal., B*, 2018, **221**, 17–26.

30 V. V. Atuchin, T. A. Gavrilova, J.-C. Grivel and V. G. Kesler, Electronic structure of layered titanate $Nd_2Ti_2O_7$, *Surf. Sci.*, 2008, **602**, 3095–3099; V. V. Atuchin, T. A. Gavrilova, J.-C. Grivel and V. G. Kesler, Electronic structure of layered ferroelectric high-*k* titanate $La_2Ti_2O_7$, *J. Phys. D: Appl. Phys.*, 2009, **42**, 035305; O. Y. Khyzhun, V. L. Bekenev, V. V. Atuchin, E. N. Galashov and V. N. Shlegel, Electronic properties of $ZnWO_4$ based on ab initio FP-LAPW band-structure calculations and X-ray spectroscopy data, *Mater. Chem. Phys.*, 2013, **140**, 558–595; V. V. Atuchin, E. N. Galashov, O. Y. Khyzhun, V. L. Bekenev, L. D. Pokrovsky, Y. A. Borovlev and V. N. Zhdankov, Low Thermal Gradient Czochralski grow thoflarge $CdWO_4$ crystals and electronic properties of (010) cleaved surface, *J. Solid State Chem.*, 2016, **236**, 24–31.

31 H. Huang, X. Han, X. Li, S. Wang, P. K. Chu and Y. Zhang, Fabrication of Multiple Heterojunctions with Tunable Visible-Light-Active Photocatalytic Reactivity in BiOBr–BiOI Full-Range Composites Based on Microstructure Modulation and Band Structures, *ACS Appl. Mater. Interfaces*, 2015, **7**, 482–492; H. Huang, X. Li, J. Wang, F. Dong, P. K. Chu, T. Zhang and Y. Zhang, Anionic Group Self-Doping as a Promising Strategy: Band-Gap Engineering and Multi-Functional Applications of High-Performance $CO_3^{2-}$-Doped $Bi_2O_2CO_3$, *ACS Catal.*, 2015, **5**, 4094–4103.

32 H. Huang, Y. He, X. Li, M. Li, C. Zeng, F. Dong, X. Du, T. Zhangd and Y. Zhang, $Bi_2O_2(OH)(NO_3)$ as a desirable

$[Bi_2O_2]^{2+}$ layered photocatalyst: strong intrinsic polarity, rational band structure and {001} active facets co-beneficial for robust photooxidation capability, *J. Mater. Chem. A*, 2015, **3**, 24547–24556.

33 H. Huang, Y. He, Z. Lin, L. Kang and Y. Zhang, Two Novel Bi-Based Borate Photocatalysts: Crystal Structure, Electronic Structure, Photoelectrochemical Properties, and Photocatalytic Activity under Simulated Solar Light Irradiation, *J. Phys. Chem. C*, 2013, **117**, 22986–22994.

34 J. Zhang, W. Yu, J. Liu and B. Liud, Illustration of high-active $Ag_2CrO_4$ photocatalyst from the first-principle calculation of electronic structures and carrier effective mass, *Appl. Surf. Sci.*, 2015, **358**, 457–462.

35 X. Li, J. Zhao and J. Yang, Semihydrogenated BN Sheet: A Promising Visible-light Driven Photocatalyst for Water Splitting, *Sci. Rep.*, 2013, **3**, 1858.

36 D. W. Hwang, J. S. Lee and W. Li, Se Hyuk Oh. Electronic Band Structure and Photocatalytic Activity of $Ln_2Ti_2O_7$ (Ln = La, Pr, Nd), *J. Phys. Chem. B*, 2003, **107**, 4963–4970.

37 C. Liu, Y. Zhang, F. Dong, A. H. Reshak, L. Ye, N. Pinna, C. Zeng, T. Zhang and H. Huang, Chlorine intercalation in graphitic carbon nitride for efficient photocatalysis, *Appl. Catal., B*, 2017, **203**, 465–474.

38 A. H. Reshak, Photocatalytic water splitting solar-to-hydrogen energy conversion: Perovskite-type hydride $XBeH_3$ (X = Li or Na) as active photocatalysts, *J. Catal.*, 2017, **351**, 119–129; A. H. Reshak, Photophysical, transport and structure properties of $Tl_{10}Hg_3Cl_{16}$ single crystals: Novel photocatalytic water-splitting solar-to-hydrogen energy conversion, *J. Catal.*, 2017, **352**, 142–154.

39 S. T. A. G. Melissen, V. Tognetti, G. Dupas, J. Jouanneau, G. Lê and L. Joubert, A DFT study of the $Al_2Cl_6$-catalyzed Friedel–Crafts acylation of phenyl aromatic compounds, *J. Mol. Model.*, 2013, **19**, 4947–4958.

40 S. Melissen, T. L. Bahers, S. N. Steinmann and P. Sautet, Relationship between Carbon Nitride Structure and Exciton Binding Energies: A DFT Perspective, *J. Phys. Chem. C*, 2015, **119**, 25188–25196.

41 A. H. Reshak and S. Auluck, Photocatalytic water-splitting solar-to-hydrogen energy conversion: Novel $LiMoO_3(IO_3)$ molybdenyl iodate based on $WO_3$-type sheets, *J. Catal.*, 2017, **351**, 1–9.

42 A. H. Reshak, Quantum Dots in Photocatalytic Applications: Efficiently Enhancing Visible Light Photocatalytic Activity by integrating CdO quantum dots as sensitizer, *Phys. Chem. Chem. Phys.*, 2017, **19**, 24915; A. H. Reshak, Active Photocatalytic Water Splitting Solar-to-Hydrogen Energy Conversion: Chalcogenide Photocatalyst $Ba_2ZnSe_3$ under Visible Irradiation, *Appl. Catal., B*, 2018, **221**, 17–26.

43 H. Huang, S. Tu, C. Zeng, T. Zhang, A. H. Reshak and Y. Zhang, Macroscopic Polarization Enhancement Promoting Photo- and Piezoelectric-Induced Charge Separation and Molecular Oxygen Activation, *Angew. Chem., Int. Ed.*, 2017, **56**, 11860–11864.

44 A. H. Reshak, S. A. Khan and S. Auluck, Electronic band structure and specific features of AA- and AB-stacking of Carbon Nitride ($C_3N_4$): DFT calculation, *RSC Adv.*, 2017, **4**, 6957–6964.

45 A. H. Reshak, S. A. Khan and S. Auluck, Linear and non-linear optical properties for AA and AB stacking of carbon nitride polymorph ($C_3N_4$), *RSC Adv.*, 2014, **4**, 11967.

46 A. H. Reshak, Thermoelectric properties for AA- and AB-stacking of Carbon Nitride polymorph ($C_3N_4$), *RSC Adv.*, 2014, **4**, 63137.

47 Q. Guo, Y. Zhang, H.-S. Zhang, Y. Liu, Y.-J. Zhao and J. G. D. Qiu, 3D Foam Strutted Graphene Carbon Nitride with Highly Stable Optoelectronic Properties, *Adv. Funct. Mater.*, 2017, **27**, 1703711.

48 P. Balaha, K. Shewartz, G. K. H. Madsen, D. Kvsnicka and J. Luitz, *WIEN2K, an Augmented plane wave + local orbitals program for calculating crystals properties, Karlheinz Schewartz*, Techn. Universitat, Wien Austria, 2001.

49 J. P. Perdew, S. Burke and M. Ernzerhof, Generalized Gradient Approximation Made Simple, *Phys. Rev. Lett.*, 1996, **77**, 3865.

50 F. Tran and P. Blaha, Accurate Band Gaps of Semiconductors and Insulators with a Semilocal Exchange–Correlation Potential, *Phys. Rev. Lett.*, 2009, **102**, 226401.

51 S. Xie, Q. Zhang, G. Liu and Y. Wang, Photocatalytic and photoelectrocatalytic reduction of $CO_2$ using heterogeneous catalysts with controlled nanostructures, *Chem. Commun.*, 2015, **52**, 35–59.

52 X. Chang, T. Wang and J. Gong, $CO_2$ photo-reduction: insights into $CO_2$ activation and reaction on surfaces of photocatalysts, *Energy Environ. Sci.*, 2016, **9**, 2177–2196.

53 P. Zhou, J. H. Wu, W. L. Yu, G. H. Zhao, G. J. Fang and S. W. Cao, Vectorial doping-promoting charge transfer in anatase $TiO_2$ {0 0 1} surface, *Appl. Surf. Sci.*, 2014, **319**, 167–172.

54 F. Wu, H. Z. Song, J. F. Jia and X. Hu, Effects of Ce, Y, and Sm doping on the thermoelectric properties of $Bi_2Te_3$ alloy, *Prog. Nat. Sci.: Mater. Int.*, 2013, **23**, 408–412.

55 X. Fan, L. Zang, M. Zhang, H. Qiu, Z. Wang, J. Yin, H. Jia, S. Pan and C. Wang, A Bulk Boron-Based Photocatalyst for Efficient Dechlorination: $K_3B_6O_{10}Br$, *Chem. Mater.*, 2014, **26**, 3169–3174.

56 J. W. Tang and J. H. Ye, Photocatalytic and photophysical properties of visible-light-driven photocatalyst $ZnBi_{12}O_{20}$, *Chem. Phys. Lett.*, 2005, **410**, 104–107.

57 J. Sato, H. Kobayashi and Y. Inoue, Photocatalytic Activity for Water Decomposition of Indates with Octahedrally Coordinated $d^{10}$ Configuration. II. Roles of Geometric and Electronic Structures, *J. Phys. Chem. B*, 2003, **107**, 7970–7975.

58 P. B. Allen, in *Quantum Theory of Real Materials*, ed. J. R. Chelikowsky and S. G. Louie, Kluwer, Boston, 1996, pp. 219–250.

59 J. M. Ziman, *Electrons and Phonons*, Clarendon, Oxford, 2001.

60 C. M. Hurd, *The Hall Effect in Metals and Alloys*, Plenum, New York, 1972.

61 G. K. H. Madsen and D. J. Singh, BoltzTraP. A code for calculating band-structure dependent quantities, *Comput. Phys. Commun.*, 2006, **175**, 67–71.

 

62 P. J. Zhou, G. Yu and M. Jaroniec, All-Solid-State Z-Scheme Photocatalytic Systems, *Adv. Mater.*, 2014, **26**, 4920–4935.
63 Q. Li, H. Meng, P. Zhou, Y. Q. Zheng, J. Wang, J. G. Yu and J. R. Gong, $Zn_{1-x}Cd_xS$ Solid Solutions with Controlled Bandgap and Enhanced Visible-Light Photocatalytic $H_2$-Production Activity, *ACS Catal.*, 2013, **3**, 882–889.
64 Q. Li, H. Meng, P. Zhou, Y. Q. Zheng, J. Wang, J. G. Yu and J. R. Gong, $Zn_{1-x}Cd_xS$ Solid Solutions with Controlled Bandgap and Enhanced Visible-Light Photocatalytic $H_2$-Production Activity, *ACS Catal.*, 2013, **3**, 882–889.
65 H. Huang, K. Xiao, N. Tian, F. Dong, T. Zhang, X. Du and Y. Zhang, Template-free precursor-surface-etching route to porous, thin g-$C_3N_4$ nanosheets for enhancing photocatalytic reduction and oxidation activity, *J. Mater. Chem. A*, 2017, **5**, 17452–17463.
66 C. Liu, H. Huang, L. Ye, S. Yu, N. Tian, X. Du, T. Zhang and Y. Zhang, Intermediate-mediated strategy to horn-like hollow mesoporous ultrathin g-$C_3N_4$ tube with spatial anisotropic charge separation for superior photocatalytic $H_2$ evolution, *Nano Energy*, 2017, **41**, 738–748.
67 N. Tian, Y. Zhang, X. Li, K. Xiao, X. Du, F. Dong, G. I. N. Waterhouse, T. Zhang and H. Huang, Precursor-reforming protocol to 3D mesoporous g-$C_3N_4$ established by ultrathin self-doped nanosheets for superior hydrogen evolution, *Nano Energy*, 2017, **38**, 72–81.
68 J. Zhang, W. Yu, J. Liu and B. Liu, Illustration of high-active $Ag_2CrO_4$ photocatalyst from the first-principle calculation of electronic structures and carrier effective mass, *Appl. Surf. Sci.*, 2015, **358**, 457–462.
69 J. C. Wu, J. W. Zheng, P. Wu and R. Xu, Study of Native Defects and Transition-Metal (Mn, Fe, Co, and Ni) Doping in a Zinc-Blende CdS Photocatalyst by DFT and Hybrid DFT Calculations, *J. Phys. Chem. C*, 2011, **115**, 5675–5682.
70 S. Banerjee, J. Gopal, P. Muraleedharan, A. K. Tyagi and B. Raj, Physics and chemistry of photocatalytic titanium dioxide: Visualization of bactericidal activity using atomic force microscopy, *Curr. Sci.*, 2006, **90**, 1378–1383.
71 J. M. Carlsson, B. Hellsing, H. S. Domingos and P. D. Bristowe, Theoretical investigation of the pure and Zn-doped α and δ phases of $Bi_2O_3$, *Phys. Rev. B: Condens. Matter Mater. Phys.*, 2002, **65**, 205122.
72 R. Hoffman, A chemical and theoretical way to look at bonding on surfaces, *Rev. Mod. Phys.*, 1988, **60**, 601.
73 C. D. Gellatt, A. R. J. Willaims and V. L. Moruzzi, Theory of bonding of transition metals to nontransition metals, *Phys. Rev. B: Condens. Matter Mater. Phys.*, 1983, **27**, 2005.
74 F. M. Gao, J. L. He, E. Wu, S. M. Liu, D. L. Yu, D. C. Li, S. Y. Zhang and Y. Tian, Hardness of Covalent Crystals, *Phys. Rev. Lett.*, 2003, **91**, 015502.